INTERNATIONAL JOURNAL FOR NUMERICAL AND ANALYTICAL METHODS IN GEOMECHANICS, VOL. 10, 569–584 (1986)

A HYBRID BOUNDARY ELEMENT–FINITE ELEMENT ANALYSIS PROCEDURE FOR FLUID FLOW SIMULATION IN FRACTURED ROCK MASSES

D. ELSWORTH

Department of Mineral Engineering, The Pennsylvania State University, University Park, Pennsylvania, U.S.A.

SUMMARY

Extension of numerical techniques to the analysis of fissure flow in three-dimensional rock masses of realistic complexity and extent constitutes an important facility in civil engineering and resource exploitation practice. Migration velocities of contaminants and fluid discharge will always be higher for a true three-dimensional network over a two-dimensional representation in that the effect of critical, out-of-plane intersections may be correctly accommodated. Revised direct boundary element formulations are developed that are capable of discretizing individual fissure discs and their intersections with adjacent fissures. Discretization coverage, by definition, is limited to the fissure edges and internal intersections, with this factor alone being a major advantage of the technique over the more conventionally utilized domain methods. Appropriate manipulation of the resulting set of equations is shown to yield a fully populated, positive definite, symmetric tensor representing the geometric conductivity of a single fissure disc. The retained degrees-of-freedom for the 'super element' are purely in terms of the fissure intersections with a minimum of 1 degree-of-freedom required per intersection. Global matrix assembly and solution is accomplished by standard finite element techniques, the global matrix being, in general, sparsely populated. The procedure is ideally suited to micro-computer solution in that a reduced degree-of-freedom system is obtained from a much larger and computationally intractable system. The advantages of boundary solution procedures are realized with minimal data input requirements and effective representation of high potential gradients. The sparsely populated and symmetric form of the global matrix retains one of the more favourable assets of the secondary finite element formulation.

INTRODUCTION

The inability of current geological exploration techniques to fully define the subsurface geometry of sparsely fractured rock masses has prompted use of stochastic modelling to generate the probable form of the inaccessible structure. From known statistical distributions of discontinuity trace length, orientation and aperture, the discontinuous nature of the rock mass may be assembled in either two- or three-dimensional representation. In this form, the mass may be numerically tested by applying known boundary conditions and evaluating numerically the discharge through the system. Such results are useful for both determining potential inflows into engineered structures within the rock mass or in determination of hydraulic conductivity tensors for specific rock mass geometries. Recent utilization of the latter of these two applications[1] has delineated the valid range of an equivalent anisotropic hydraulic conductivity tensor in homogenizing the performance of a discrete system. For certain systems of limited spatial extent, the discrete nature of the discontinuous networks of fissures may result in the system never attaining an equivalent

0363–9061/86/060569–16$08.00

Received 11 February 1985
Revised 23 July 1985

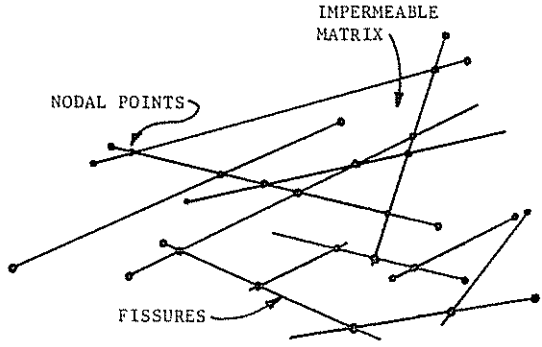

Figure 1. An idealized two-dimensional geometry for intersecting fissures

anisotropic hydraulic conductivity. In these instances, evaluation of discharges into a proposed excavation would require that the full discrete system is modelled numerically.

Where it is required that the system is represented as a discrete network of interconnected fissures, the number of unknowns involved within the analysis is likely to become intractable as both the density of fissure coverage and spatial limits of the domain are increased. This is most dramatically apparent where extension is made from two-dimensional representation of a fissure networks to the three-dimensional case. For two-dimensional analysis, as illustrated in Figure 1, each fissure is assumed of constant aperture with the head distribution between nodes being linear. This situation dictates that no advantage in computational accuracy is achieved by locating nodes at positions other than at fissure intersections. In three dimensions, however, this is clearly not the case since the pattern of flow applicable to the geometry illustrated in Figure 2 cannot easily be reduced to a simplified form. In this instance, the geometric conductivity of the unit is an intrinsic function of the relative geometry of the fissure disc external and internal boundaries. The external boundary corresponds to the no-flow edge of the fissure and the internal boundaries the intersections with other fissures.

Clearly, if it is possible to represent the geometric conductivity of a single fissure disc purely in terms of the lines of intersection with other fissures, the storage requirements for a three-dimensional fissure network of realistic dimensions could be retained within a practical limit. It is this motivation that has prompted the following.

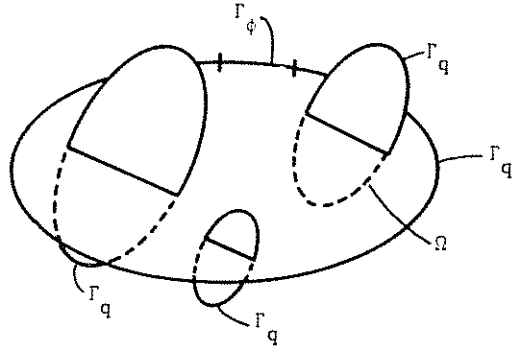

Figure 2. Intersecting fissure discs in a three-dimensional representation of a rock mass

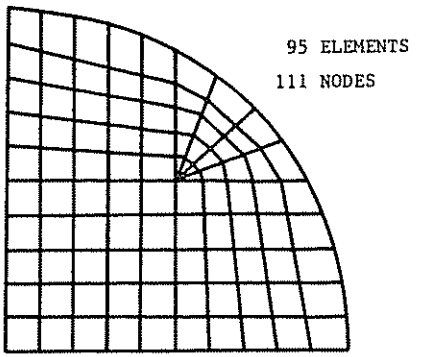

Figure 3. Finite element mesh for a single quadrant of a porous disc

SOLUTION ALTERNATIVES

The finite element method may be applied to the problem where elements require to be meshed within the plane of the fissure as illustrated in Figure 3. The nature of the problem dictates that meshing should be densest adjacent to the tips of the intersections with other fissures in order to accurately reproduce the high velocity and head gradients. Once meshed, the geometry may be condensed by conventional techniques to yield a unit of reduced degree-of-freedom. This unit would be the equivalent of a substructure in structural mechanics.

For a problem geometry of this form, automatic mesh generation and refinement procedures would be required together with automated routines for static condensation. This is considered overly cumbersome and computationally expensive with another alternative being sought for this case.

Solution to this problem in semi-analytical form has been proposed,[1] where matched image sinks and sources are used to create the appropriate no-flow boundary condition on the external edge of the fissure. The proposed method assembles appropriate terms into a global matrix relating hydraulic discharge to changes in head. The resulting matrix is sparsely populated but nonsymmetric and conforms to a finite difference method of solution.

An alternative solution to the problem may be realized if boundary solution[2] procedures are invoked. Boundary elements may be discretized along the trace of the external fissure edge and along the lines of intersection with other fissures. The reduced elemental coverage required in this respect is evident in Figure 2. Imposing appropriate boundary conditions to the assemblage and rearranging the unknowns yields an elemental geometric conductivity matrix of minimum order equal to the number of intersections. The matrix is, by definition, positive definite, symmetric and fully populated at the elemental level. The following discusses the problem formulation.

GOVERNING EQUATIONS FOR INTEGRAL SOLUTION

For linear potential flow within a domain (Ω) bounded by a surface (Γ), the boundary constraint equation may be stated in generality as[3,4]

$$c(p)\phi(p) + \int_\Gamma V(p,q)\phi(q)\,\mathrm{d}\Gamma = \int_\Gamma \Phi(p,q)v(q)\cdot\bar{n}\,\mathrm{d}\Gamma \tag{1}$$

where $V(p,q)$ and $\Phi(p,q)$ are kernel functions relating, respectively, to velocities and potentials at point (q) on the boundary of the domain due to a unit point source at (p) internally. The terms $v(q)$

and $\phi(q)$ are velocities of flow and potential heads at (q) and are either prescribed as boundary conditions or unknowns that require evaluation. The domain outer normal is denoted as $\bar{n}$ and $c(p)$ represents a dimensionless scalar applied to the free term, being a function of the domain geometry at (p). If the internal point (p) is enclosed entirely within the domain (Ω), then $c(p)$ is equal to unity. If (p) is moved to the boundary, then $c(p) = \frac{1}{2}\delta_{pq}$ if the boundary is smooth, where δ_{pq} is the Kronecker delta.[5]

For plane flow problems involving only the (x_1, x_2) plane, the appropriate kernel functions are for a line source of strength (M) within an infinite medium. The relevant expressions for these are given as[6]

$$\Phi(p,q) = \frac{M}{2\pi} \ln r; \qquad V(p,q)_r = \frac{-KM}{2\pi r} \tag{2a,b}$$

where K is the fissure conductivity and r the radial separation of the source and point of consideration (p to q). For laminar flow within a fissure of constant aperture (b), the hydraulic conductivity derived from the parallel plate flow analogy is

$$K = \frac{gb^2}{12\nu} \tag{3}$$

where g is the gravitational acceleration and ν is the kinematic viscosity of the fluid.

The kernels Φ and V appear in equation (1) under the term of integration and are evaluated using quadrature in this application. Two separate cases are considered, where (i) straight boundary elements with constant weighting function distribution and (ii) curved boundary elements with quadratic variation of basis function are used, respectively. The straight-line elements may be defined as super-parametric with respect to geometry[7] and the curved elements isoparametric. Isoparametric formulation of equation (1) is the more general case and discussion will be restricted

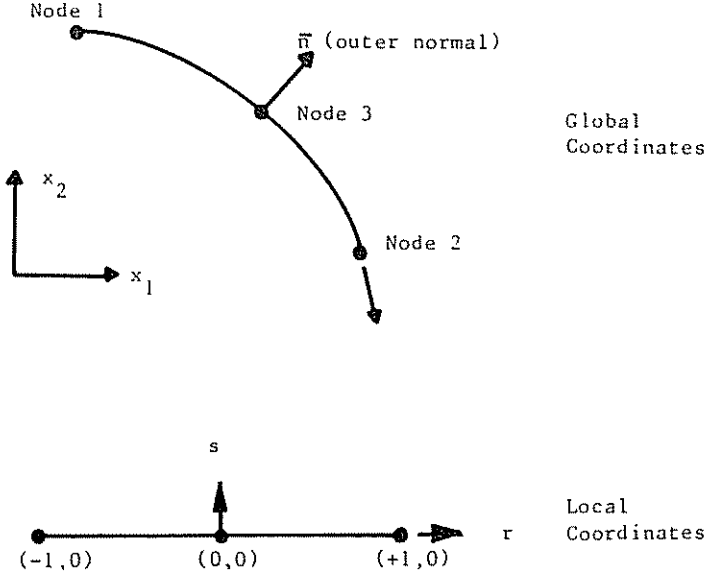

Figure 4. Element geometry for isoparametric formulation

to this facet. The straight-line elements represent a specific subclass of this more universal formulation.

General isoparametric formulation

Lagrangian basis functions are used to represent both geometry and integration intensity for the terms in equation (1). The geometric configuration of a single element in global and natural co-ordinates is illustrated in Figure 4. The vector of basis functions (**h**) is defined as

$$\mathbf{h}^{\mathrm{T}} = \tfrac{1}{2}[(1-r)-(1-r^2);(1+r)-(1-r^2);2(1-r^2)] \tag{4}$$

where r represents the intrinsic co-ordinates of the bi-unit element. By substitution

$$x_1 = \mathbf{h}^{\mathrm{T}}\mathbf{x}_1; \qquad x_2 = \mathbf{h}^{\mathrm{T}}\mathbf{x}_2$$
$$\phi = \mathbf{h}^{\mathrm{T}}\boldsymbol{\phi}; \qquad v\cdot\bar{n} = \mathbf{h}^{\mathrm{T}}\mathbf{v}\cdot\bar{\mathbf{n}} \tag{5a,b,c,d}$$

where non-vectoral quantitities ($x_1, x_2, \phi, v\cdot\bar{n}$) are co-ordinates and variables, respectively, and vectoral terms ($\mathbf{x}_1, \mathbf{x}_2, \boldsymbol{\phi}, \mathbf{v}\cdot\bar{\mathbf{n}}$) are the nodal magnitudes of these parameters. The terms in equation (1) are most conveniently integrated by quadrature over the extent of the bi-unit element where the revised expression may be stated as

$$c(p)\phi(p) + \int_{-1}^{+1} V(p,q)\phi(q)\frac{\mathrm{d}\Gamma}{\mathrm{d}r}\,\mathrm{d}r = \int_{-1}^{+1} \Phi(p,q)v(q)\cdot\bar{n}\frac{\mathrm{d}\Gamma}{\mathrm{d}r}\,\mathrm{d}r \tag{6}$$

and the Jacobian for the mapping, for this one-dimensional reduction, is given as

$$\frac{\mathrm{d}\Gamma}{\mathrm{d}r} = \left[\left(\frac{\mathrm{d}x_1}{\mathrm{d}r}\right)^2 + \left(\frac{\mathrm{d}x_2}{\mathrm{d}r}\right)^2\right]^{1/2} \tag{7}$$

Appropriate substitutions of equations (5c, d) into (6) may be made with the terms of equation (7) being determined from the derivatives of the basis function vector such that

$$\frac{\mathrm{d}}{\mathrm{d}r}(x_1) = \frac{\mathrm{d}}{\mathrm{d}r}(\mathbf{h}^{\mathrm{T}})\mathbf{x}_2 = \mathbf{h}'^{\mathrm{T}}\mathbf{x}_1 \text{ etc.} \tag{8}$$

and

$$\mathbf{h}'^{\mathrm{T}} = [(r-\tfrac{1}{2});(r+\tfrac{1}{2});-2r] \tag{9}$$

The unit outward normal of the system may be evaluated from equation (9) in a straightforward manner. The final form of equation (6) may then be evaluated by Gaussian quadrature. Two-point quadrature[8] has proved effective in the evaluation of all integrals except those in which the unit point source is located within the element. For these specific cases the $V(p,q)$ and $\Phi(p,q)$ integrals are unbounded in the range of integration. The natural logarithm within the $\Phi(p,q)$ kernel may be evaluated from special quadrature formulae[9] where suitable changes of variable are invoked. The unbounded term of the $V(p,q)$ kernel, in association with the free term $c(p)$, may be evaluated from consideration of mass conservation over the domain boundary. A direct analogy may be drawn between this procedure and consideration of rigid body translations in elastostatic applications.[5,10]

The above formulation renders the boundary constraint equation in the most general format for three-noded isoparametric elements. Identical procedures may be invoked for line elements of constant basis function where a single central node is defined. For this case, appropriate substitution into equations 5(a, b) and 5(c, d) are

$$\mathbf{h}^{\mathrm{T}} = \tfrac{1}{2}[(1-r);(1+r)] \qquad \text{and} \qquad \mathbf{h}^{\mathrm{T}} = 1{\cdot}0 \tag{10a, b}$$

respectively. The vector of basis function derivatives is therefore

$$\mathbf{h}'^{\mathrm{T}} = [-1/2; +1/2] \tag{11}$$

Evaluation of equation (6) results in a system of n simultaneous equations where the mixed Dirichlet and Neumann boundary conditions provide n known terms. For either the super-parametric (i) or isoparametric (ii) cases, n represents the number of nodes describing parameter variation within the solution domain.

Slit element formulation

The general procedure outlined above is suitable for representing the external fissure boundary without further modification. For slit elements representing the intersection of fissure discs, allowance must be made for flow into the slit from either side. A typical circular fissure disc containing twin slits symmetrically disposed about the horizontal axis is illustrated in Figure 5.

It is possible to mesh boundary elements on the contour of the slit to completely enclose an internal void. This option is less than satisfactory in that the proximity of adjacent elements results in both poor solution accuracy and added nodal degrees-of-freedom. This shortcoming may be circumvented if special slit elements are used to represent the internal boundaries whereby a single element may be meshed on the internal boundary. Two procedures may be used to develop such elements. A dipole analogy with electrostatics may be utilized where twin sources of identical polarity and magnitude are brought together to an infinitesimal separation. Alternatively, an inductive proof may be used whereby a perforated plate containing an annulus of finite dimension is collapsed to a linear form. The pertinent details of each proof are contained within Appendix I.

Regardless of the procedures employed to define the form of the slit elements, the resulting integrals are identical. As might be expected, the terms corresponding to the left-hand side of equation (1) directly accommodate an appropriate free term ($c(p)$) equal to unity. This is consistent with the slit elements being entirely enclosed within the external boundary discretization.

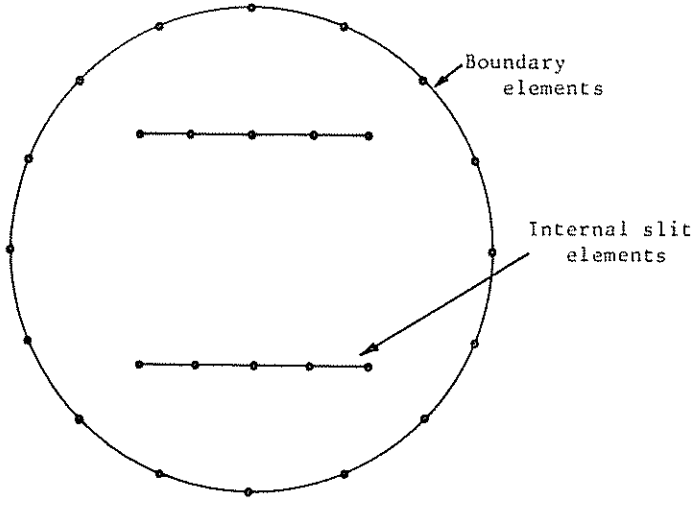

Figure 5. A single circular fissure disc intersected by two other fissure discs

BOUNDARY CONDITIONS

Assembly of equation (6) renders a matrix expression of the form

$$\underset{n\times n}{\mathbf{V}}\ \underset{n\times 1}{\boldsymbol{\phi}} = \underset{n\times n}{\boldsymbol{\Phi}}\ \underset{n\times 1}{\mathbf{v}} \tag{12}$$

where $\mathbf{V}$ and $\boldsymbol{\Phi}$ are matrices containing the integrated kernel terms and $\boldsymbol{\phi}$ and $\mathbf{v}$ are nodal parameters of hydraulic potential and normal velocity.

Boundary conditions consistent with the disc geometry must be imposed prior to solution. The normal (to the boundary) velocity is zero over the external edge of the fissure and conditions of constant, but unknown, hydraulic potential are imposed on the internal slits. Those may be stated as

$$v\cdot\bar{n} = 0 \qquad \in\Gamma_q \tag{13}$$

$$\phi = \text{constant} \qquad \in\Gamma_\phi \tag{14}$$

where Γ_q and Γ_ϕ represent the external and internal extents of the perforated fissure disc. Appropriate column interchanges within the matrix form of equation (1) yields a system of n equations where n represents the total number of system nodes. Applying the known Neumann boundary conditions of equation (13) results in the number of solution cases equal to the number of internal nodes. The solution process may be presented symbolically as

$$\mathbf{v} = [\mathbf{V}^{-1}\boldsymbol{\Phi}]\boldsymbol{\phi}; \qquad \mathbf{v} = \mathbf{K}\boldsymbol{\phi} \tag{15}$$

where the bracketed term represents a geometric conductance matrix which is, by definition, positive definite and symmetric.

For multiple fissure discs of differing aperture, and hence hydraulic conductivity, the expression must be modified to enforce discharge continuity at internal nodes such that

$$\mathbf{q} = b\int_{\Gamma_\phi} \mathbf{h}^{\mathrm{T}}\mathbf{v}\cdot\bar{\mathbf{n}}\,\mathrm{d}\Gamma \tag{16}$$

where q is the discharge rate, b the nominal fissure aperture along the slit element and the remaining terms are as previously defined. The matrix then conforms directly to finite element format and may be assembled into a sparsely populated global matrix for multiply connected fissure systems according to standard finite element procedure.

NUMBER OF NUMERICAL OPERATIONS

Although the necessity of performing a matrix inversion is inferred by equation (15), this inversion is symbolic and may be more efficiently accomplished by standard elimination procedures. For the case of an elemental disc comprising a total of n nodes with m of these on internal slits, the solution procedure may be shown to be equivalent to solving a system of n equations for m different boundary conditions. Thus the total number of operations in obtaining the condensed conductivity tensor are of the order of

$$\tfrac{1}{2}n^3 + n^2 m$$

All reductions are at the elemental level prior to global matrix assembly. Manageable small systems of equations are therefore maintained. Each slit must be represented by a minimum of a single degree-of-freedom, although there is no sensible maximum restriction to the number of degrees-of-freedom retained per slit.

With the number of numerical operations retained at this level, efficiency is comparable to that obtained through static condensation procedures for pre-processing of finite element analyses. One important advantage the procedure retains over finite element analyses is the ability to dispense with complex automated mesh generation and refinement techniques. Where some hundreds of fissures may be required in a typical representation of a rock mass, the usefulness of this facility may be clearly envisaged.

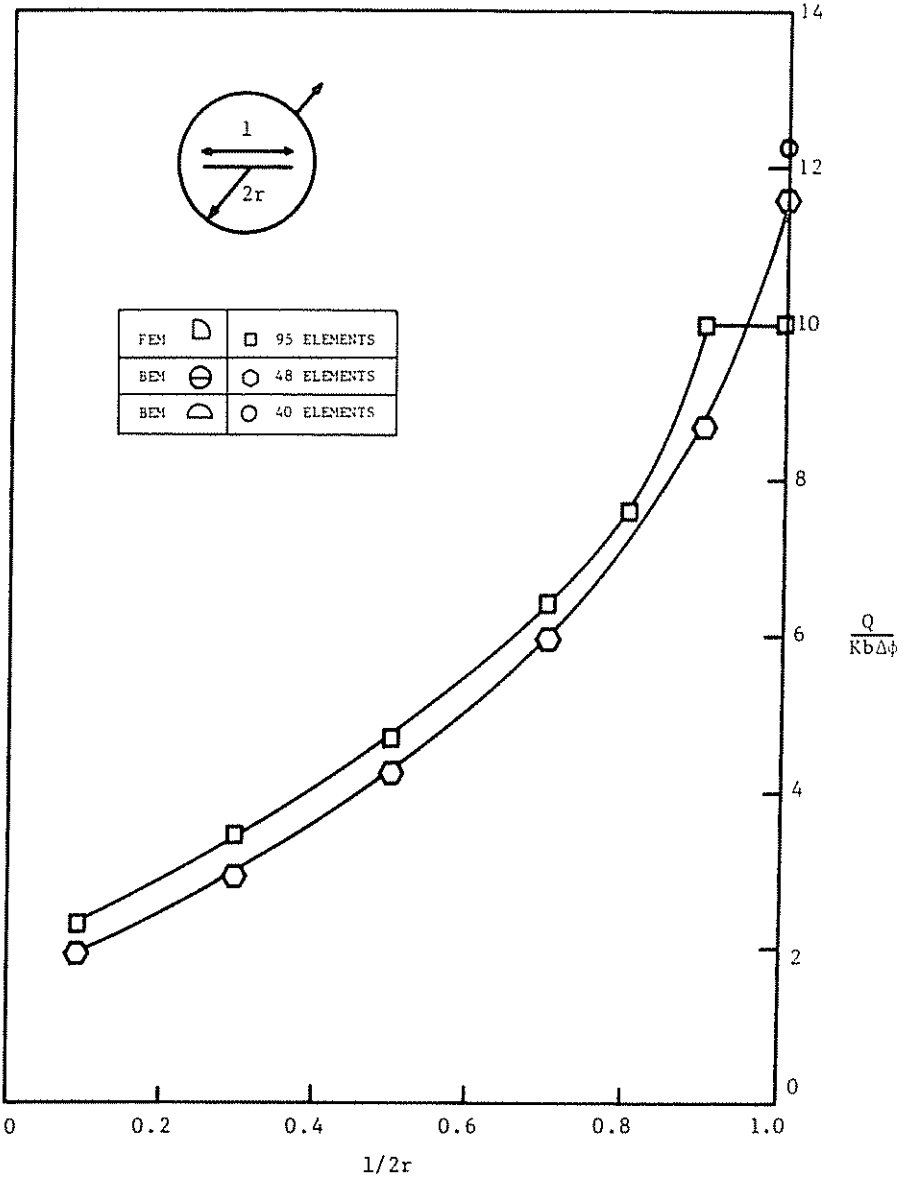

Figure 6. Dimensionless discharges from a circular disc containing a single centrally located slit with an open boundary. Super-parametric representation

VALIDATION

Validation has been completed for a number of different boundary condition geometries against finite element solution. The relative efficiency and accuracy of both super-parametric and isoparametric forms are examined. The finite element mesh is shown in Figure 3 for quarter symmetry. The mesh comprises 95 constant flow velocity elements and 111 nodes. Meshing is arranged with greatest density in the area adjacent to the fissure intersection tip to faithfully reproduce the anticipated high head gradients. Owing to the use of another numerical solution

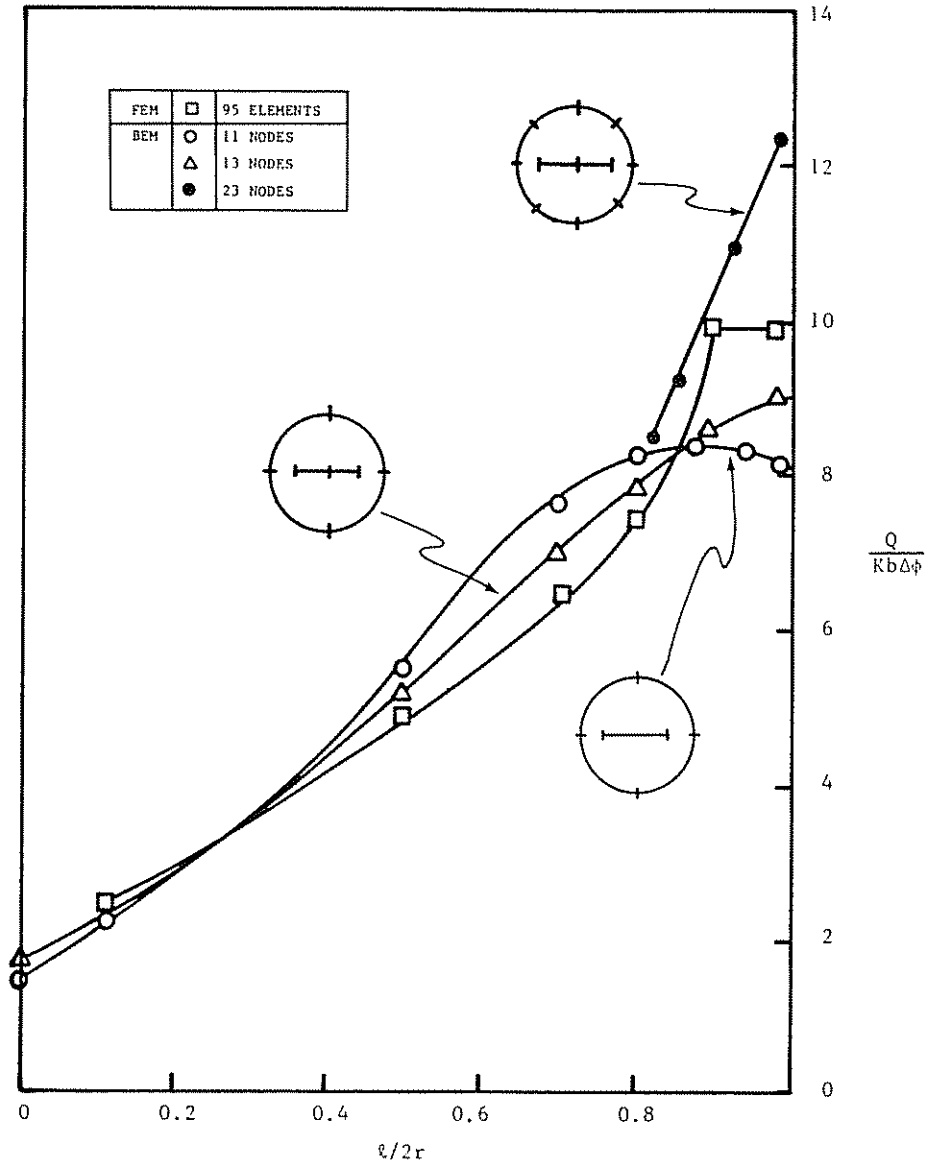

Figure 7. Dimensionless discharges from a circular disc containing a single centrally located slit with an open boundary. Isoparametric representation

technique to check the boundary solution method, comparison of the results may only be regarded in a non-absolute sense. Indeed, the boundary element formulation is anticipated to more faithfully represent the occurrence of high head gradients adjacent to the crack tip.

For a single slit located centrally within a circular disc, the dimensionless discharges under conditions of uniform external head are shown in Figure 6 for the super-parametric formulation. The slit length to disc diameter ratio ($l/2r$) is increased to unity for a fully traversing slit. Close agreement is evident between the two solution procedures, even for a fully traversing slit.

The performance of the higher order isoparametric elements is illustrated in Figure 7. Excellent agreement is achieved with minimal element density. An initial system comprising eleven unknowns is shown to provide satisfactory results for length to diameter ratios ($l/2r$) as high as 0·8. Increased coverage beyond this bound appears desirable up to the case of a fully traversing slit. The superiority of the isoparametric formulation is apparent in reducing the number of equations for any required degree of precision.

Dimensionless average entry velocities (v/K) into the slit are shown in Figure 8, from which it is evident that the boundary element formulation is better conditioned to reproduce the high gradients close to the slit ends. Even for the case of 12 external boundary elements and four single-noded slit elements, the results give discharges in close agreement to those for the higher elemental coverage. This particular solution represents an instance of only 16 unknowns. The excellent agreement returned for this minimal elemental coverage is clear testimony as to the potential of the method. For a fully traversing single slit, the variation in dimensionless velocity (v/K) is given for both solution procedures in Figure 9. In this instance, the boundary element formulations may be utilized both for slit elements and merely by meshing unmodified boundary

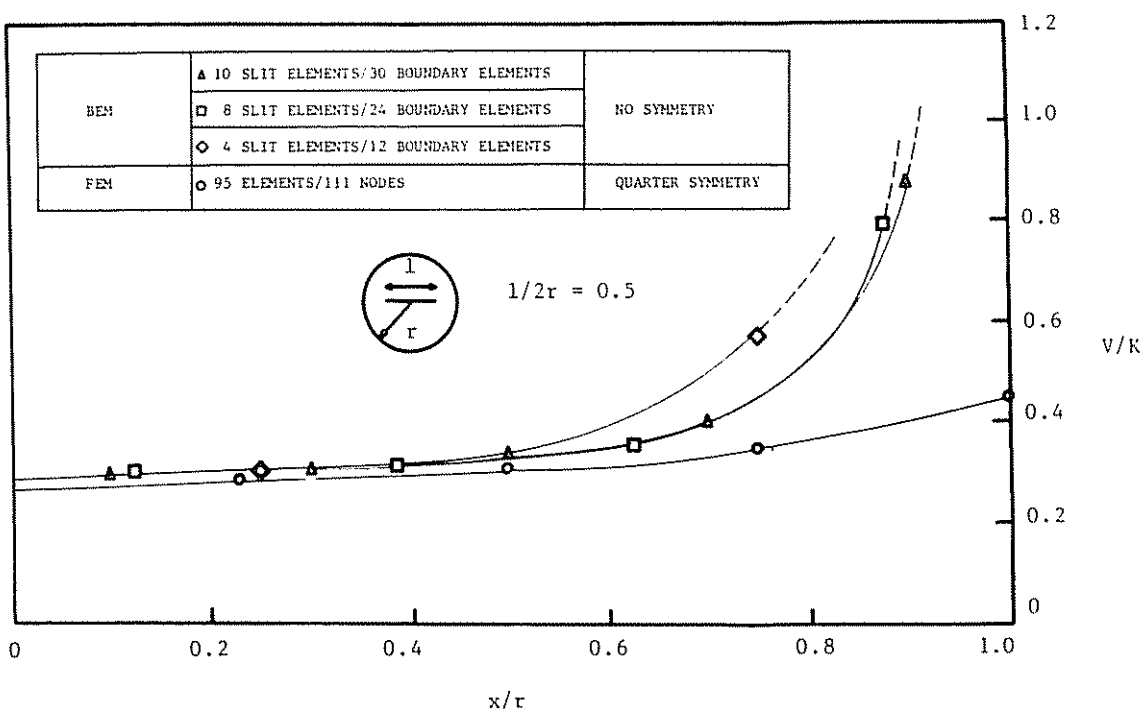

Figure 8. Entry velocities along the length of a partially traversing slit element

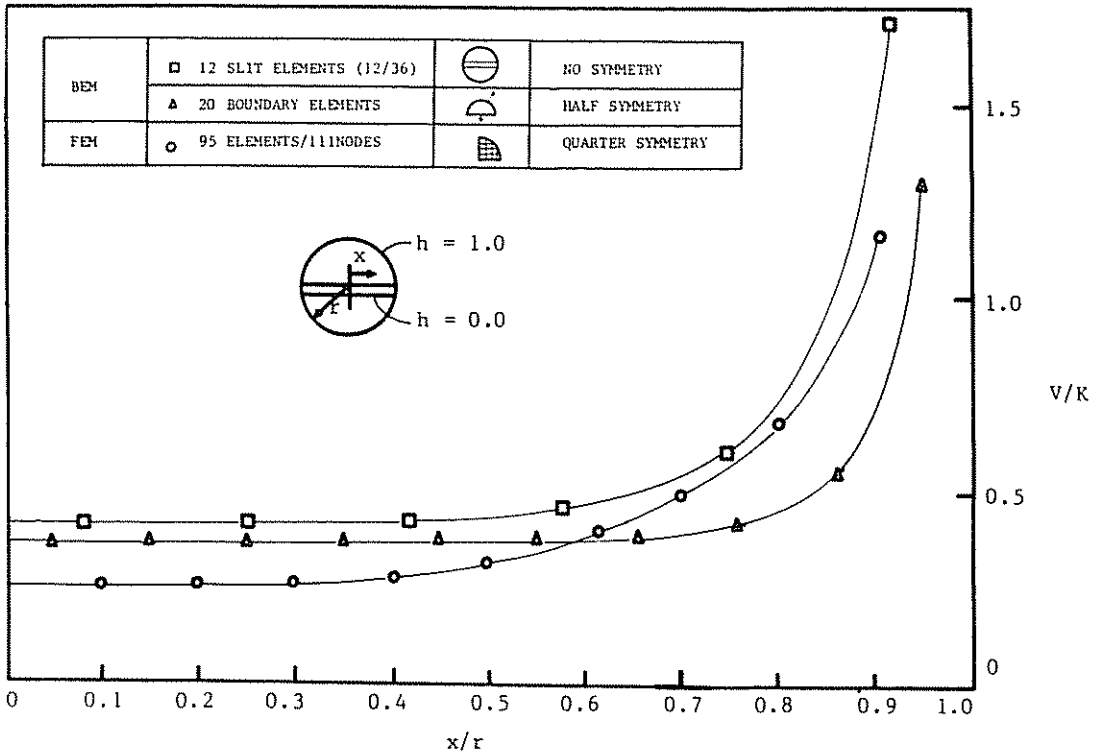

Figure 9. Entry velocities along the length of a fully traversing slit element

Table I. Dimensionless discharges for a disc cut by twin, fully traversing slits

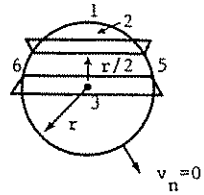

NUMBER OF NODES PER SEGMENT						$\frac{Q}{Kb\Delta\phi}$	FORMULATION
1	2	3	4	5	6		
4	2	2	6	1	1	3·90422	Super-parametric
8	4	4	12	2	2	3·85980	Super-parametric
8	8	8	12	2	2	3·95124	Super-parametric
—	4	4	—	2	2	3·80541	Super-parametric
—	8	8	—	4	4	3·80530	Super-parametric
FEM—95 ELEMENTS						3·77565	
5	5	5	9	3	3	3·78966	Isoparametric
5	7	7	9	3	3	3·79898	Isoparametric
3	5	5	5	2	2	3·97891	Isoparametric
3	3	3	5	2	2	4·04462	Isoparametric

elements along the slit axis. These two different concepts are illustrated in the figure key. Both solution procedures are shown to give comparable results.

For the case where multiple slits are involved, comparison of the two solution procedures yield close agreement. The variation in dimensionless parameters for solution by the different formulations is given in Table I for fully traversing slits. Results for partially traversing slits are

Table II. Dimensionless discharges for a disc cut by twin, partially traversing slits

$\ell/2r_1 = 0.5$

$r_1/r_2 = 2.0$

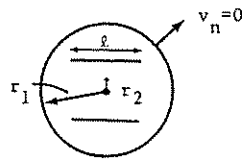

NODE COVERAGE ON EXTERNAL/SLIT 1/SLIT 2	$\frac{Q}{Kb\Delta\phi}$	FORMULATION
24/4/4	1·53978	Super-parametric
20/5/5	1·55107	Super-parametric
48/8/8	1·56149	Super-parametric
FEM—95 ELEMENTS	1·54007	
8/6/6	1·70391	Isoparametric
16/5/5	1·64561	Isoparametric
32/9/9	1·6099	Isoparametric

given in Table II. In all cases, the results fall within a narrow band, the absence of an appropriate analytical solution making it impossible to make judgement with respect to relative accuracy in an absolute sense.

From the foregoing, it is evident that the proposed method is capable of yielding accurate determinations of fissure geometric conductivities for relatively modest discretization densities. It is appropriate, at this stage, to illustrate the potential applicability with an example.

FISSURE NETWORK EXAMPLE

The flexibility of the proposed solution procedure may be most graphically illustrated by a simple example geometry. A network consisting of six elliptical discs is chosen. Disc semi-major axis to semi-minor axis ratios of 2·0 and 3·5 are chosen, the geometry of the network being illustrated in Figure 10. Following reduction of individual discs, a single degree-of-freedom is retained per intersection, resulting in a total of 8 degrees-of-freedom for the system.

Although the system is relatively simple, essentially comprising two subsystems in parallel, variation in the transmissivities of individual discs yields some instructive results. Figure 11 illustrates the effect on the dimensionless discharge of adjusting individual disc transmissivities. Three specific cases are examined, T_i referring to the transmissivity of disc i and $T_{i,j,k}$ symbolically representing the series transmissivity of discs i, j and k. Transmissivity is defined as the product of hydraulic conductivity and nominal fissure aperture. Three important permutations of this

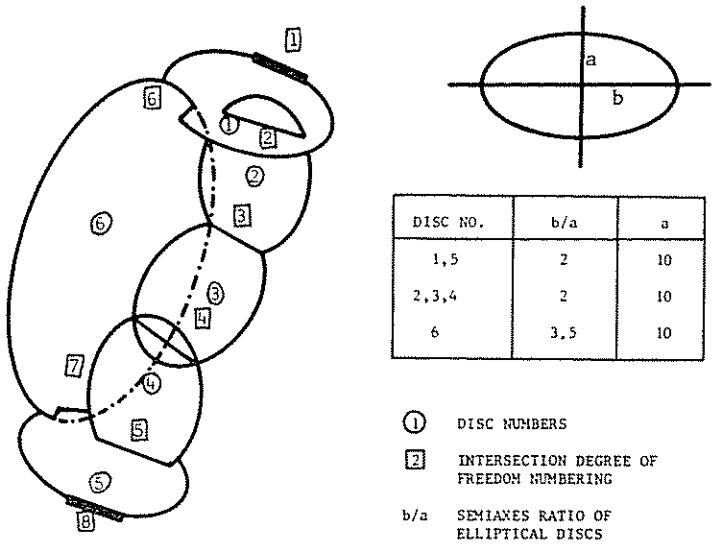

Figure 10. A closed system of elliptical discs

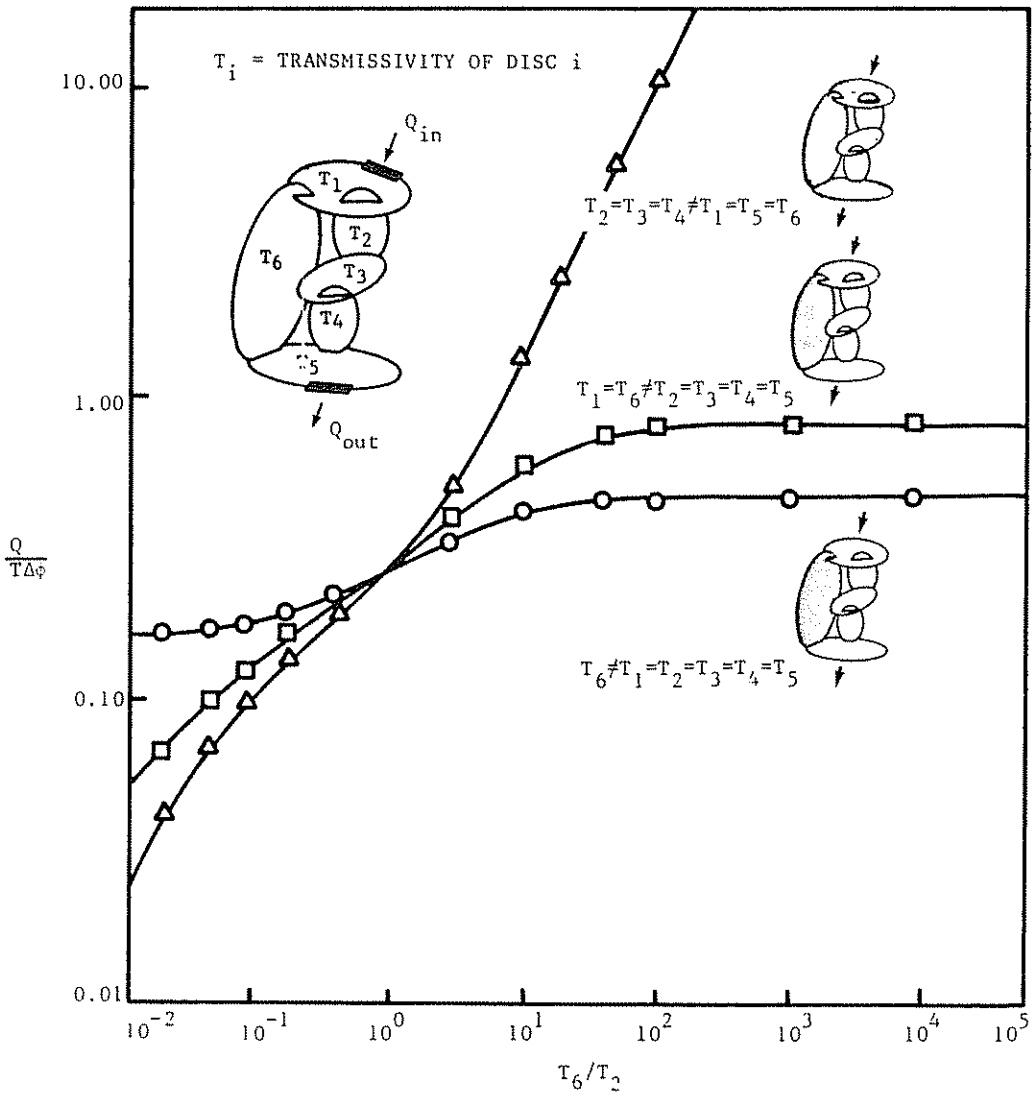

Figure 11. Dimensionless discharge from the three-dimensional disc assemblage for various disc transmissivity ratios

system may be identified as follows:

(i) Isolated fracture of different nominal transmissivity (T_6)

At very low transmissivity of fissure 6, minimal contribution to the global flow is made by that disc. The system conductivity reflects the behaviour with disc 6 removed, i.e. ($T_{1,2,3,4,5}$).

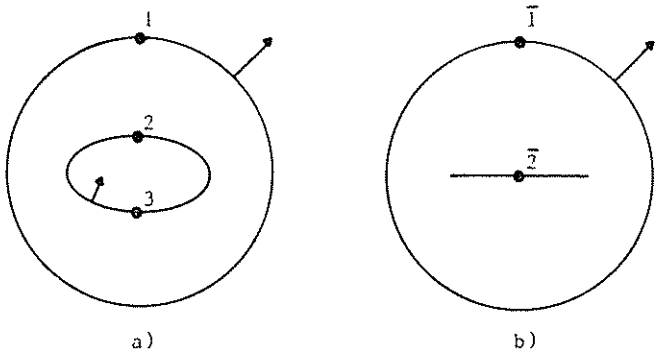

Figure 12. Schematic illustration of a 3-noded disc assemblage in (a) uncollapsed and (b) collapsed representations

As T_6 is increased, the contribution to the system conductivity increases, but asymptotes to a steady value controlled by entry and exit discs 1 and 5, i.e. ($T_{1,5}$). A near perfect hydraulic connection exists between degrees-of-freedom 6 and 7.

(ii) Isolated fractures of different nominal transmissivity (T_1, T_6)

At low transmissivities of fissures 1 and 6, the flow through the system is controlled by the impedence of fissure 1. The dimensionless flow rate is directly proportional to T_1 and no asymptote can be reached. For high transmissivities of $T_{1,6}$, the flow is controlled by T_5 which remains constant. The resulting steady flow asymptote corresponds to a steady discharge given by T_5.

(iii) Continuous system of fractures of different nominal transmissivity (T_1, T_5, T_6)

In this instance, the system of fractures fully encase the remainder of the network and thus dominate the behaviour. When the encasing system transmissivity is very low, the transmission properties are controlled directly by $T_{1,5}$. At high transmissivities for fissures 1, 5 and 6, this system provides a complete flow path of extremely high conductance and consequently dominates the hydraulic behaviour.

The above illustrate the 'weakest link' behaviour of the system and the effect of this on the fluid discharge. The existence of extensive fissures of large aperture are therefore illustrated to have a controlling influence in short-circuiting flow paths. It is important to note, however, that even for the case of short circuiting conduits, some control of the behaviour is maintained by the smaller less conductive fissures. This is especially apparent where less conductive fractures skirt the zone of supply or withdrawal, as in this example.

CONCLUSIONS

For large, three-dimensional representations of fissured rock masses, conventional finite element analyses are rendered intractable. In plane meshing of elements dictates that for a network of 100 fissures with 100 nodes per fissure, the number of system unknowns is of the order 10^4. The large system of equations may be reduced by condensation techniques, although there are specific advantages associated with using a revised boundary element formulation, as follows: (i) only the fissure edge and the lines of intersection with other fissures require to be discretized; (ii) using this discretization, the velocity singularities at the tips of the intersection slits are more meaningfully accommodated than with conventional finite element models; (iii) for domains of large volume to surface area ratio, the solution technique may be regarded as of superior efficiency to finite element analysis; (iv) all numerical reductions are at the elemental level involving small systems of equations that may be adequately preprocessed by mini- or micro-computer; (v) the resulting elemental conductivity matrix is positive definite, symmetric and conforms to conventional finite element formulation; (vi) the global conductance matrix is sparsely populated.

Boundary solution procedures are illustrated to perform well with relatively sparing elemental coverage. Although the super-parametric formulation performs adequately, isoparametric representation is shown to be slightly superior in efficiency. The true representation of the curved external form of the fissure discs is likely to be the most important contributing factor in this regard. The curved elements therefore represent a more consistent solution to the problem. Two-point quadrature was found to be adequate in evaluating the integrals of kernel functions, even in instances where slit elements fully penetrated discs.

It is concluded, therefore, that the numerical procedure proposed herein provides a tractable method of simulating potential flow in spatially large realizations of fractured rock masses.

ACKNOWLEDGEMENTS

This work was supported by the Director's Development Fund of Lawrence Berkeley Laboratory and by the Natural Science and Engineering Research Council of Canada under Grant A-3-642-187-50.

APPENDIX I

Identities to represent slit elements may be developed either from inductive reasoning or from a more formal basis if a dipole analogy is invoked. For the former of these, consider the initial three-noded assemblage of Figure 12(a). The statement of the boundary constraint equation for this case may be defined in indicial form as

$$V_{ij}\phi_j = \Phi_{ij}v_j \tag{17}$$

where V_{ij} represents the influence of the velocity kernel source at node i on node j. The velocity term (v_j) is the component normal to the boundary. If the annulus is collapsed as in Figure 12(b), then the following matrix identities may be discerned by inspection in the limit such that

$$V_{21} = V_{31}; V_{12} = -V_{13} \tag{18}$$

$$V_{22} = V_{33} = V_{23} = V_{32} \tag{19}$$

$$\Phi_{12} = \Phi_{13}; \Phi_{21} = \Phi_{31} \tag{20}$$

$$\Phi_{23} = \Phi_{32} = \Phi_{22} = \Phi_{33} \tag{21}$$

Nodal variables for the collapsed form may be identified as

$$\bar{\phi}_2 = \phi_2 = \phi_3 \tag{22}$$

$$\bar{v}_2 = v_2 + v_3 \tag{23}$$

with the bar denoting variables for the revised numbering of Figure 12(b). Appropriate substitution of (18)–(23) into (17) and summing rows 2 and 3 yields the identity

$$\begin{bmatrix} V_{11} & 0 \\ V_{21} & 2V_{22} \end{bmatrix} \begin{Bmatrix} \phi_1 \\ \bar{\phi}_2 \end{Bmatrix} = \begin{bmatrix} \Phi_{11} & \Phi_{12} \\ \Phi_{21} & \phi_{22} \end{bmatrix} \begin{Bmatrix} v_1 \\ \bar{v}_2 \end{Bmatrix} \tag{24}$$

which represents the revised statement of the boundary constraint equation. The matrix statement may be obtained for multiple internal slits by similar reasoning.

An analogy may be drawn between the concept of a dipole as used in electrostatics[6] where twin sources are brought to constant strength with separation. This analogy using point forces of opposing polarity has been used successfully in elastostatic applications,[11] although this formulation requires that sources of identical polarity are used.

The velocity of flow at point $i(v_i)$ induced by a single line source at point j may be evaluated from equation (2b) as a function or radius $f(r)$ such that

$$v_i = Mf(r) \tag{25}$$

where M is the source strength. If twin sources are disposed symmetrically about the $(x_2 = 0)$ axis at total infinitesimal separation equal to $2a$, then the induced radial velocity of flow at point (i), referenced to the $(x_2 = 0)$ axis is

$$v_i = M\left\{f - \frac{\partial f}{\partial x_2} + f + \frac{\partial f}{\partial x_2}\right\} = 2Mf(r) \tag{26}$$

and similarly for total hydraulic potential (ϕ_i)

$$\phi_i = 2Mf(r) \tag{27}$$

This result corresponds to the final form obtained by induction in equation (24) if it is remembered that $\bar{v}_2 = v_2 + v_3$ in equation (23). These results have been used in both super-parametric and isoparametric formulations reported previously.

REFERENCES

1. J. C. S. Long, 'Investigation of equivalent porous medium permeability in networks of discontinuous fractures', *Ph.D. thesis*, Univ. of California, Berkeley (1983).
2. P. K. Banerjee and R. Butterfield, *Boundary Element Methods in Engineering Science*, McGraw-Hill, London, 1981.
3. M. A. Jawson, 'Integral equation methods in potential theory: I', *Proc. Roy. Soc. A*, **275**, 23–32 (1963).
4. G. T. Sym, 'Integral equation methods in potential theory: II', *Proc. Roy. Soc. A*, **275**, 33–46 (1963).
5. T. A. Cruse, 'An improved boundary-integral equation method for three dimensional elastic stress analysis', *Comp. Struct.*, **4**, 741–754 (1974).
6. O. D. Kellog, *Foundations of Potential Theory*, Dover, New York, 1953.
7. O. C. Zienkiewicz, *The Finite Element Method*, 3rd edn, McGraw-Hill, London, 1977.
8. A. H. Stroud and D. Secrest, *Gaussian Quadrature Formulas*, Prentice-Hall, New York, 1966.
9. D. G. Anderson, 'Gaussian quadrature formulate for $\int = \ln(x) f(x)\,dx$', *Math. Comp.*, **19**, 477–481 (1965).
10. J. C. Lachat and J. O. Watson, 'Effective numerical treatment of boundary integral equations: a formulation for three-dimensional elastostatics', *Int. j. numer. methods eng.*, **10**, 991–1005 (1976).
11. B. H. G. Brady and J. W. Bray, 'The boundary element method for elastic analysis of tabular orebody extraction, assuming complete plane strain', *Int. J. Rock Mechs. Min. Sci.*, **15**, 29–37 (1978).